

Electron-atom bremsstrahlung: double differential cross section and polarization correlations

Vladimir A. Yerokhin^{1,2,3} and Andrey Surzhykov^{1,2}

¹*Institute of Physics, University of Heidelberg, Philosophenweg 12, D-69120 Heidelberg, Germany*

²*Gesellschaft für Schwerionenforschung, Planckstraße 1, D-64291 Darmstadt, Germany*

³*Center for Advanced Studies, St. Petersburg State Polytechnical University, Polytekhnicheskaya 29, St. Petersburg 195251, Russia*

The leading-order electron-atom bremsstrahlung is investigated within the rigorous relativistic approach based on the partial-wave representation of the Dirac wave functions in the external atomic field. Approximating the atomic target by an effective local potential, we calculate the double-differential cross section and the polarization correlations in a wide range of the impact energies. Connection between the bremsstrahlung at the hard-photon end point of the spectrum and the continuum-threshold limit of the radiative recombination is studied. A detailed analysis of the screening effect and the energy dependence of the polarization correlations is presented, with the main focus on the high impact energy region.

PACS numbers: 34.80.-i, 34.50.-s, 41.60.-m, 78.70.En

I. INTRODUCTION

Bremsstrahlung, the emission of a photon by an electron scattering from an atom, is one of the fundamental processes that occur in the electron-atom collisions. For a large region of the impact energies of the incoming electron, the atom can be well represented by a static central (screening) potential, thus ignoring the exchange interaction between the incoming electron and the target and virtual excitations of the target. The corresponding approximation is sometimes referred as the “ordinary” bremsstrahlung mechanism, to distinguish from the so-called “polarization” bremsstrahlung, in which the excess energy is transferred to the target and the photon is emitted from the atomic core. The polarization bremsstrahlung is the dominant mechanism in, e.g., the *proton-atom* collisions (see, e.g., Ref. [1]), where the ordinary bremsstrahlung is suppressed by the small electron-to-proton mass ratio. In the electron-atom collisions, however, the polarization mechanism is usually not significant for the not-too-small energies of the incoming electron.

Within the screening-potential approximation, the bremsstrahlung process can be described rigorously (to the leading order in the fine-structure constant α) within the exact relativistic approach based on the partial-wave representation of the Dirac continuum electron states with a fixed value of the asymptotic momentum. This approach is clearly preferable as compared to numerous approximate treatments reported in the literature but it is also more difficult for practical implementations. The partial-wave decomposition of the initial and final electron states, together with the multipole expansion of the wave function of the emitted photon, lead to a large number of expansion terms that have to be summed up until convergence is reached. Despite technical difficulties encountered, the first partial-wave expansion calculations were reported already in 1960s [2, 3]. The first accurate

numerical results were obtained by Tseng and Pratt in 1970s. In a series of calculations [4–7], they reported results for the single- and double-differential cross sections for a wide interval of the impact energies. Polarization correlations in the double-differential cross section were studied in Ref. [8]. More recently, several calculations of the triple-differential cross section and the corresponding polarization correlations were performed [9–11].

Experimental investigations of the electron-atom bremsstrahlung, numerous in 1960s and 1970s [12], became rather sparse during the following decades. In the last years, however, advent of a new generation of the Compton polarimeters [13] revived the experimental interest to bremsstrahlung. In particular, it became possible to perform experiments with the spin-polarized electrons, which opens up new vistas for experimental studies of various correlations between the polarizations of the incoming electron and the emitted photon. Such experiments are currently underway in Gesellschaft für Schwerionenforschung (GSI) [14] and Technical University of Darmstadt [15].

Because of the experimental limitations in the past, the previous bremsstrahlung calculations were focused mainly on the cross sections. The only detailed partial-wave expansion study of the polarization correlations was accomplished by Tseng and Pratt [8]. Detailed as it is, this calculation is not sufficient to cover all present experimental needs. In particular, the region of the impact energies $E > 500$ keV, presently available for the experimental investigation in GSI, has not been carefully investigated in that work. Besides this, the results reported in Ref. [8] have never been carefully checked by an independent calculation. In the present investigation, we aim to cover this gap by checking and extending the previous bremsstrahlung results by Tseng and Pratt.

The paper is organized as follows. In Sec. II, we present relativistic formulas for the double-differential bremsstrahlung cross section and polarization correlations, obtained within the density-matrix formalism.

Sec. III describes the numerical approach used in this work. In Sec. IV we discuss the connection between the bremsstrahlung at the hard-photon end point of the spectrum and the continuum-threshold limit of the radiative recombination. Numerical results are presented and discussed in Sec. V.

The relativistic units ($\hbar = c = 1$) are used throughout this paper.

II. THEORY

In the present investigation we consider the bremsstrahlung of an electron scattering from an atom, which is represented by a static central potential. The scattered electron in the final state is assumed to be not observed. The kinematics of the process is defined as follows. The reference frame is the rest frame of the atom. The z axis is directed along the asymptotic momentum of the incident electron \mathbf{p}_i . The xz plane (also referred to as the *reaction* plane) is defined by \mathbf{p}_i and the momentum of emitted photon \mathbf{k} . In this frame, the direction of the emitted photon is defined just by the polar angle θ_k , $\cos \theta_k = \hat{\mathbf{p}}_i \cdot \hat{\mathbf{k}}$, where $\hat{\mathbf{x}} \equiv \mathbf{x}/|\mathbf{x}|$.

In order to study the polarization correlations between the incident electron and the emitted photon, we express the density matrix of the final state $\langle \mathbf{k}\lambda | \rho_f | \mathbf{k}\lambda' \rangle^1$ in terms of the initial-state density matrix as

$$\begin{aligned} \langle \mathbf{k}\lambda | \rho_f | \mathbf{k}\lambda' \rangle &= \sum_{m_i m'_i m_f} \int d\Omega_f \langle \mathbf{p}_i m_i | \boldsymbol{\alpha} \cdot \hat{\mathbf{u}}_\lambda e^{i\mathbf{k}\cdot\mathbf{r}} | \mathbf{p}_f m_f \rangle^* \\ &\times \langle \mathbf{p}_i m'_i | \boldsymbol{\alpha} \cdot \hat{\mathbf{u}}_{\lambda'} e^{i\mathbf{k}\cdot\mathbf{r}} | \mathbf{p}_f m_f \rangle \langle \mathbf{p}_i m_i | \rho_i | \mathbf{p}_i m'_i \rangle, \end{aligned} \quad (1)$$

where \mathbf{p}_i , m_i (m'_i) and \mathbf{p}_f , m_f are the asymptotic momentum and the spin projection of the incident and scattered electron states, respectively; \mathbf{k} and λ (λ') are the momentum and the helicity of the emitted photon ($\lambda = \pm 1$), $\hat{\mathbf{u}}_\lambda$ is the unit polarization vector of the photon, and Ω_f is the solid angle of the scattered electron. The energy of the emitted photon $k \equiv |\mathbf{k}|$ is fixed by $k = \varepsilon_i - \varepsilon_f$, where $\varepsilon_n = \sqrt{p_n^2 + m^2}$.

The advantage of the present formulation is that the density matrix (1) contains the full information about the polarization properties of the emitted photon (see, e.g., Ref. [16]),

$$\langle \mathbf{k}\lambda | \rho_f | \mathbf{k}\lambda' \rangle = \frac{1}{2} \text{Tr} [\rho_f] \begin{pmatrix} 1 + P_3 & P_1 - iP_2 \\ P_1 + iP_2 & 1 - P_3 \end{pmatrix}, \quad (2)$$

where P_i are the Stokes parameters. We note that the sign of the Stokes parameters depends on the definition of

the circular polarization unit vectors, see Eq. (14) below and the text after it. The trace of the density matrix is, up to a prefactor, the double-differential cross section summed over all photon polarizations. Following Ref. [4], we introduce the normalized cross section $\sigma(k)$ as

$$\begin{aligned} \sigma(k) &\equiv \frac{k}{Z^2} \frac{d\sigma}{dk} = 2\pi \int_{-1}^1 d(\cos \theta_k) \frac{k}{Z^2} \frac{d\sigma}{dk d\Omega_k} \\ &= \frac{1}{32\pi} \frac{k^2}{p_i^2} \frac{\alpha}{Z^2} \int_{-1}^1 d(\cos \theta_k) \text{Tr} [\rho_f], \end{aligned} \quad (3)$$

where Z is the nuclear charge of the target atom and the continuum electron wave function is assumed to be normalized on the energy scale.

The Stokes parameters P_1 and P_2 describe the linear polarization of the emitted photon. They can be determined experimentally by measuring the intensities I_ϕ of the linearly polarized photon emission at different angles ϕ with respect to the reaction plane,

$$P_1 = \frac{I_{0^\circ} - I_{90^\circ}}{I_{0^\circ} + I_{90^\circ}}, \quad (4)$$

$$P_2 = \frac{I_{45^\circ} - I_{135^\circ}}{I_{45^\circ} + I_{135^\circ}}. \quad (5)$$

Instead of the P_1 and P_2 parameters, it is often convenient to describe the linear polarization by the polarization ellipse in the plane perpendicular to the photon momentum \mathbf{k} . The ellipse is defined by the relative length of the principal axis P_L which reflects the degree of the linear polarization,

$$P_L = \sqrt{P_1^2 + P_2^2}, \quad (6)$$

and the tilt angle χ ,

$$\chi = \frac{1}{2} \arctan \frac{P_2}{P_1}. \quad (7)$$

The Stokes parameter P_3 defines the degree of the circular polarization of the emitted photon,

$$P_3 = \frac{W(+1) - W(-1)}{W(+1) + W(-1)}, \quad (8)$$

where $W(+1)$ and $W(-1)$ are weights of the right- and left-polarized photons, respectively.

We now turn to the evaluation of Eq. (1). The initial-state density matrix is represented in terms of the spherical tensors $\rho_\kappa^{(i)}$ of rank $\kappa = 0$ and 1 as [16]

$$\langle \mathbf{p}_i m_i | \rho_i | \mathbf{p}_i m'_i \rangle = \sum_{\kappa q} (-1)^{1/2 - m'_i} C_{1/2 m_i, 1/2 - m'_i}^{\kappa q} \rho_{\kappa q}^{(i)}. \quad (9)$$

The components of $\rho_\kappa^{(i)}$ are expressed in terms of the polarization vector of the incoming electron $P_i = (P_x, P_y, P_z)$ as

$$\rho_{00}^{(i)} = \frac{1}{\sqrt{2}}, \quad \rho_{10}^{(i)} = \frac{1}{\sqrt{2}} P_z, \quad \rho_{1\pm 1}^{(i)} = \mp \frac{1}{2} (P_x \mp iP_y). \quad (10)$$

¹ More exactly, this is the reduced density matrix of the emitted photons, with the quantum numbers of the (unobserved) final-state electron traced out. In the context of the present paper, we refer to it just as the density matrix of the final state.

The spherical-wave decomposition of the ingoing (+) and outgoing (−) continuum electron wave function with a definite asymptotic momentum is [17]

$$|\mathbf{p}m\rangle = 4\pi \sum_{\kappa\mu} i^l e^{\pm i\Delta_\kappa} C_{lm_i, \frac{1}{2}m}^{j\mu} Y_{lm_i}^*(\hat{\mathbf{p}}) |\varepsilon\kappa\mu\rangle, \quad (11)$$

where $j = |\kappa| - 1/2$, $l = |\kappa + 1/2| - 1/2$, $\Delta_\kappa = \sigma_\kappa + (l + 1)\pi/2$, and σ_κ is the asymptotic phase of the wave function, see Eq. (13) below. The function $|\varepsilon\kappa\mu\rangle$ is the Dirac eigenstate with the energy $\varepsilon = \sqrt{p^2 + m^2}$, the relativistic angular quantum number κ , and the angular momentum projection μ , represented by

$$|\varepsilon\kappa\mu\rangle = \begin{pmatrix} g_{\varepsilon,\kappa}(r) \chi_{\kappa\mu}(\hat{\mathbf{r}}) \\ i f_{\varepsilon,\kappa}(r) \chi_{-\kappa\mu}(\hat{\mathbf{r}}) \end{pmatrix}, \quad (12)$$

where g and f are the upper and lower radial components, respectively, and $\chi_{\kappa\mu}$ are the spherical spinors [18]. The wave function is normalized on the energy scale and its asymptotic (as $r \rightarrow \infty$) behavior is

$$g_{\varepsilon,\kappa}(r) \simeq \frac{1}{r} \left(\frac{\varepsilon + m}{\pi p} \right)^{1/2} \cos[pr + \sigma_\kappa + \eta \ln(2pr)], \quad (13)$$

where $\eta = Z_\infty \alpha \varepsilon / p$, and Z_∞ is the effective nuclear charge of the atom at large distances, $Z_\infty = \lim_{r \rightarrow \infty} r V_{\text{scr}}(r)$, with V_{scr} being the atomic potential.

The spherical-wave decomposition of the photon field with the helicity (circular polarization) $\lambda = \pm 1$ is

$$\hat{\mathbf{u}}_\lambda e^{i\mathbf{k}\cdot\mathbf{r}} = \sqrt{2\pi} \sum_{LMp} i^L \sqrt{2L+1} (i\lambda)^p \mathbf{a}_{LM}^{(p)}(\hat{\mathbf{r}}) D_{M\lambda}^L(\hat{\mathbf{k}}), \quad (14)$$

where the components of the circular-polarization vector $\hat{\mathbf{u}}_\lambda$ are defined as [18] $u_1 = (u_x + iu_y)/\sqrt{2}$ and $u_{-1} = (u_x - iu_y)/\sqrt{2}$, $D_{M\lambda}^L$ is Wigner's D function [19], $\mathbf{a}_{LM}^{(p)}$ are the magnetic ($p = 0$) and electric ($p = 1$) vectors defined by

$$\mathbf{a}_{LM}^{(0)}(\hat{\mathbf{r}}) = j_L(kr) \mathbf{Y}_{LLM}(\hat{\mathbf{r}}), \quad (15)$$

$$\begin{aligned} \mathbf{a}_{LM}^{(1)}(\hat{\mathbf{r}}) &= j_{L-1}(kr) \sqrt{\frac{L+1}{2L+1}} \mathbf{Y}_{L L-1 M}(\hat{\mathbf{r}}) \\ &\quad - j_{L+1}(kr) \sqrt{\frac{L}{2L+1}} \mathbf{Y}_{L L+1 M}(\hat{\mathbf{r}}), \end{aligned} \quad (16)$$

\mathbf{Y}_{JLM} is the vector spherical harmonics [19],

$$\mathbf{Y}_{JLM}(\hat{\mathbf{r}}) = \sum_{m\sigma} C_{Lm,1\sigma}^{JM} Y_{Lm}(\hat{\mathbf{r}}) \mathbf{e}_\sigma, \quad (17)$$

and \mathbf{e}_σ is the spherical component of the unity vector.

Inserting expansions (9), (11) and (14) into Eq. (1) and employing the standard angular-momentum technique, we arrive at

$$\begin{aligned} \langle \mathbf{k}\lambda | \rho_f | \mathbf{k}\lambda' \rangle &= 8(2\pi)^4 \sum_{\kappa_i \kappa'_i \kappa_f} \sum_{LL' \kappa g t} \sum_{\gamma_1 \gamma_2} D_{\gamma_1 \gamma_2}^g(\hat{\mathbf{k}}) \rho_{\kappa, -\gamma_1}^{(i)} i^{l_i - l'_i - L + L'} e^{i\Delta_{\kappa_i} - i\Delta_{\kappa'_i}} [L, L', j_i, j'_i, l_i, l'_i, g, \kappa]^{1/2} \\ &\quad \times (-1)^{j'_i - j_f + l_i + g + \kappa} C_{L'\lambda', L-\lambda}^{g\gamma_2} C_{l_i 0, l'_i 0}^{t0} C_{g-\gamma_1, \kappa \gamma_1}^{t0} \begin{Bmatrix} L & j_f & j_i \\ j'_i & g & L' \end{Bmatrix} \begin{Bmatrix} 1/2 & 1/2 & \kappa \\ j'_i & j_i & g \\ l'_i & l_i & t \end{Bmatrix} \\ &\quad \times \sum_{pp'} (-i\lambda)^p (i\lambda')^{p'} \langle \varepsilon_i \kappa_i | \boldsymbol{\alpha} \cdot \mathbf{a}_L^{(p)} | \varepsilon_f \kappa_f \rangle^* \langle \varepsilon_i \kappa'_i | \boldsymbol{\alpha} \cdot \mathbf{a}_{L'}^{(p')} | \varepsilon_f \kappa_f \rangle, \end{aligned} \quad (18)$$

where $[x_1, x_2, \dots] \equiv (2x_1 + 1)(2x_2 + 1) \dots$, $l_a = |\kappa_a + 1/2| - 1/2$, $l'_a = |\kappa_a - 1/2| - 1/2$, $j_a = |\kappa_a| - 1/2$, and the reduced matrix elements are evaluated in Appendix A.

In this work, we will present our results in terms of the differential cross section and the Stokes parameters of the emitted photon as functions of the polarization vector of the incident electron: $\sigma(P_x, P_y, P_z)$, $P_1(P_x, P_y, P_z)$, $P_2(P_x, P_y, P_z)$, and $P_3(P_x, P_y, P_z)$. We consider four choices of the polarization of the incident electron: (i) unpolarized, $(P_x, P_y, P_z) = (0, 0, 0)$; (ii) polarized transversely within the reaction plane, $(P_x, P_y, P_z) = (1, 0, 0)$; (iii) polarized perpendicularly to the reaction plane $(P_x, P_y, P_z) = (0, 1, 0)$; and (iv) longitudinally polarized, $(P_x, P_y, P_z) = (0, 0, 1)$. Not all of

the polarization correlations for these 4 choices are independent and nonvanishing. Properties of the angular-momentum coefficients in Eq. (18) lead to the following identities,

$$P_1(0, 0, 0) = P_1(1, 0, 0) = P_1(0, 0, 1), \quad (19)$$

$$P_2(0, 0, 0) = P_2(0, 1, 0) = 0, \quad (20)$$

$$P_3(0, 0, 0) = P_3(0, 1, 0) = 0, \quad (21)$$

$$d\sigma(0, 0, 0) = d\sigma(1, 0, 0) = d\sigma(0, 0, 1), \quad (22)$$

where $d\sigma(P_x, P_y, P_z) \equiv (k/Z^2) d\sigma(P_x, P_y, P_z)/(dk d\Omega_k)$. Taking into account the above identities leaves us with 8 independent quantities to be calculated: $d\sigma(0, 0, 0)$, $d\sigma(0, 1, 0)$, $P_1(0, 0, 0)$, $P_1(0, 1, 0)$, $P_2(1, 0, 0)$, $P_2(0, 0, 1)$,

$P_3(1, 0, 0)$, and $P_3(0, 0, 1)$.

In previous calculations reported in the literature, the polarization correlations were often parameterized in terms of the coefficients C_{ij} introduced by Tseng and Pratt [8]. In order to simplify comparison with previous studies, we give the list of correspondence between the coefficients C_{ij} and the present notations,

$$C_{03} = P_1(0, 0, 0), \quad (23)$$

$$C_{11} = -P_2(1, 0, 0), \quad (24)$$

$$C_{12} = -P_3(1, 0, 0), \quad (25)$$

$$C_{23} = P_1(0, 0, 0) - P_1(0, 1, 0), \quad (26)$$

$$C_{31} = P_2(0, 0, 1), \quad (27)$$

$$C_{32} = P_3(0, 0, 1), \quad (28)$$

$$C_{20} = 1 - \frac{d\sigma(0, 1, 0)}{d\sigma(0, 0, 0)}. \quad (29)$$

III. NUMERICAL CALCULATION

The problem of calculating the final-state density matrix (18) is now reduced to the evaluation of the radial integrals and the summation over the angular-momentum and multipole quantum numbers. The radial integrals to be evaluated are

$$J_l^{12}(a, b) = \int_0^\infty dr r^2 g_{\varepsilon_a, \kappa_a}(r) f_{\varepsilon_b, \kappa_b}(r) j_l(kr), \quad (30)$$

$$J_l^{21}(a, b) = \int_0^\infty dr r^2 f_{\varepsilon_a, \kappa_a}(r) g_{\varepsilon_b, \kappa_b}(r) j_l(kr), \quad (31)$$

where g and f are the radial components of the continuum Dirac wave function and j_l is the spherical Bessel function. A straightforward numerical evaluation of these radial integrals is problematic since all three functions in the integrand are highly oscillating and slowly decreasing for large values of r .

Several methods were reported in the literature for evaluation of such highly oscillatory integrals. For the case of the point-Coulomb potential, the integrals can be evaluated analytically in terms of the Appel functions of three complex variables [2, 20]. Weak points of this method are, first, the restriction to the particular choice of the atomic potential and, second, the absence of reliable numerical methods for evaluation of the Appel functions for a wide range of parameters and arguments.

The method used in calculations by Tseng and Pratt [4, 8] is based on dividing the integration region $(0, \infty)$ into two parts, the inner and the outer ones, in such a way that the wave function in the outer region can be approximated by the (phase-shifted) free-field solutions. In the inner part, the Dirac equation is solved and the radial integrations are performed numerically. In the outer region, the analytical form of the free-field solution is exploited and the radial integrals are performed by the so-called integration by parts method, which was never described in the literature [21].

In the present work, the radial integrals are evaluated numerically after rotating the integration contour in the complex r plane. For the first time this elegant method was used probably in Ref. [22], in connection with nuclear collision problems. For the case of the integrals involving three spherical Bessel functions, this method was studied in detail in Ref. [23]. Integrals involving the nonrelativistic Coulomb functions and negative powers of the radial coordinate were investigated in Ref. [24]. More recently, the complex-plane rotation method was used in calculations of the $(e, 2e)$ process [25] and the Compton scattering [26]. In the present work, we extend the complex-plane integration method to the case of the Dirac Coulomb wave functions. The calculational scheme is described in detail in Appendices B and C. This method allowed us to evaluate the radial integrals required up to typically 9-digit precision.

The continuum-state wave functions for the general case of the screening potential were obtained by numerical solution of the Dirac equation with help of the RADIAL package by Salvat et al. [27]. For the point-Coulomb potential, we used the analytical representation for the Dirac eigenstates in terms of the Whittaker functions, see Eqs. (B2) and (B3). The Whittaker M and W functions were evaluated by a generalization of our codes developed in Ref. [28].

In the present work, we perform calculations for two choices of the atomic potential: (i) the point-nucleus Coulomb potential and (ii) the screening potential of a neutral atom. The screening potential was constructed as

$$V_{\text{scr}}(r) = V_{\text{nuc}}(r) + \alpha \int_0^{R_0} dr' \frac{1}{\max(r, r')} \rho(r'), \quad (32)$$

where V_{nuc} is the potential of the (extended-size) nucleus, R_0 is the radius of the atom, and $\rho(r)$ is the radial electron density of atomic orbitals normalized by

$$\int_0^{R_0} dr \rho(r) = Z. \quad (33)$$

The radial atomic electron density was calculated by the multiconfigurational Dirac-Fock method by using the GRASP package [29]. We note that the previous calculations by Tseng and Pratt [4, 8] used a somewhat simpler model of the screening potential, which included only a local part of the exchange interaction between the atomic electrons.

Once the radial integrals are successfully evaluated, the main problem in numerical calculation is to ensure the convergence of the multiple sum in Eq. (18). When all tri-angular selection rules are taken into account, two summations remain unbound, which can be chosen to be $|\kappa_i|$ and $|\kappa_f|$. The convergence properties of the sum depend strongly both on the kinetic energy of the incoming electron E and on the fractional part of it carried away by the photon, k/E . The convergence is fast for $E < 1$ MeV and close to the hard photon end of the spectrum (the tip region, $k/E \sim 1$) and becomes rather slow for larger impact

energies and(or) near the soft photon end. In the tip region, the expansion over the final-state quantum number $|\kappa_f|$ converges rapidly, so that a non-symmetric partial-wave cutoff is appropriate. Our calculations in this region included up to $(n_i, n_f) = (80, 10)$ partial waves. Further away from the tip region, we used the symmetric configurations up to $(n_i, n_f) = (55, 55)$ partial waves, with further extension being complicated by numerical instabilities.

IV. CONNECTION BETWEEN BREMSSTRAHLUNG AND RADIATIVE RECOMBINATION

From the general physical point of view, it is natural to expect a relation between the bremsstrahlung (BS) at the hard photon end of the spectrum (the tip region), where the electron transfers all its kinetic energy to the photon, and the radiative recombination (RR) into highly excited atomic states. This connection was studied previously by a number of authors [30–33]. Approaching the tip region from the continuum side was investigated in Ref. [34]. In this work, we would like to demonstrate the connection between these two processes by explicit numerical calculations.

For the Stokes parameters, the connection between RR and BS is most transparent. It can be observed that, for RR into atomic states with a given angular momentum quantum number κ , the Stokes parameters have a well-defined limit as the principal quantum number $n \rightarrow \infty$. In order to make a connection to BS, one has to account for the recombination into subshells with different values of κ (for a fixed value of n) and then evaluate the limit of $n \rightarrow \infty$. More specifically, the RR Stokes parameter P_1 is extrapolated to the continuum threshold as

$$P_1^{\text{tip}} = \lim_{n \rightarrow \infty} \frac{\sum_{\kappa} [I_{0^\circ}(n\kappa) - I_{90^\circ}(n\kappa)]}{\sum_{\kappa} [I_{0^\circ}(n\kappa) + I_{90^\circ}(n\kappa)]}, \quad (34)$$

where $I_\chi(n\kappa)$ denotes the intensity of the photons emitted under angle χ in RR of an electron into a bound atomic substate $|n\kappa\rangle$. For explicit formulas and details on $I_\chi(n\kappa)$, we refer the reader to the recent review by Eichler and Stöhlker [17]. The other Stokes parameters P_2 and P_3 are obtained analogously to Eq. (34), by using Eqs. (5) and (8).

In actual calculations, the limit $n \rightarrow \infty$ was evaluated by going to sufficiently high values of n (typically, $n \approx 15 - 20$), whereas the summation over κ was restricted to a few terms. (The s , p , d , f , and g waves were taken into account.)

A somewhat different procedure is required for approaching the continuum threshold limit in the case of the cross section. It is well-known that the cross section of RR into the individual Rydberg states falls off as $\sim n^{-3}$. Making a connection to the BS [33], one should take into account that the individual levels cannot be resolved experimentally as $n \rightarrow \infty$. The measured quantity

depends on the resolution of the photon detector Δk and is given by

$$\left\langle \frac{d\sigma_{\kappa}^{\text{RR}}}{d\Omega_k} \right\rangle_{\Delta k} = \frac{1}{\Delta k} \sum_{n \geq n_0} \frac{d\sigma_{n\kappa}^{\text{RR}}}{d\Omega_k}, \quad (35)$$

where $\sigma_{n\kappa}^{\text{RR}}$ is the cross section of RR into an individual level with given n and κ and n_0 is defined by the condition that the binding energy $E_{n_0} = \Delta k$. In order to approach the continuum threshold, we sum over κ and take the limit $n_0 \rightarrow \infty$,

$$\frac{d^2\sigma^{\text{tip}}}{dk d\Omega_k} = \lim_{n_0 \rightarrow \infty} \left(\frac{1}{\Delta k(n_0)} \sum_{n \geq n_0} \sum_{\kappa} \frac{d\sigma_{n\kappa}^{\text{RR}}}{d\Omega_k} \right). \quad (36)$$

In the limit $n \rightarrow \infty$, one can use the nonrelativistic expression for the binding energy, $\Delta k(n) = m(Z\alpha)^2/(2n^2)$, and the well-known asymptotic behavior of the RR cross section, $d\sigma_{n\kappa}^{\text{RR}}/d\Omega_k = A_\kappa(\theta)/n^3$, with the result

$$\frac{d^2\sigma^{\text{tip}}}{dk d\Omega_k} = \sum_{\kappa} \frac{A_\kappa(\theta)}{m(Z\alpha)^2}. \quad (37)$$

In our calculations, we determine the parameter $A_\kappa(\theta)$ by fitting the RR cross sections calculated for a series of n , to the $1/n^3$ scaling law.

Fig. 1 illustrates the connection between BS and RR, as obtained in our numerical calculations for the double differential cross section and the Stokes parameters in the case of the point Coulomb potential. We observe good agreement in all cases; the small remaining deviation is attributed to extrapolation errors. It is important that our RR and BS calculations are completely independent of each other. The BS calculation is performed as described in this work, whereas the RR calculation is carried out as reported in Ref. [35], with the radial integrations performed analytically. So, the agreement observed is also as an important cross-check between two different calculational approaches.

V. RESULTS AND DISCUSSION

We begin this section by comparing our numerical results with those obtained in the best previous partial-wave expansion calculations by Tseng and Pratt [4, 8]. Table I presents comparison for the bremsstrahlung cross section $\sigma(k)$ given by Eq. (3) for the gold target, both for the Coulomb and screening potentials. We observe excellent agreement between the calculations performed for the Coulomb potential. For the screening potential, all our results are by about 1% smaller than the ones by Tseng and Pratt. This difference is apparently due to a more realistic screening potential used in this work [see the discussion after Eq. (33)]. Results of the two calculations for the double differential cross section and for all independent polarization corrections C_{ij} [see Eqs. (23)–(29)] are compared in Fig. 2 for the case of the Coulomb

potential. We find nearly perfect agreement in all cases. As a matter of fact, the agreement observed is quite remarkable, taking into account that the calculation by Tseng and Pratt was accomplished four decades ago.

In Fig. 3, we study the effect of the screening on the cross section and the Stokes parameter P_1 for the initially unpolarized electrons. First of all, we observe that the sign of the effect varies: the screening reduces the cross section but increases the Stokes parameters. For the cross section, the screening effect depends strongly on the nuclear charge Z . The effect is barely recognizable (in the region of energies studied) for carbon, while for gold, it is significant for all energies.

It is interesting to observe that the bremsstrahlung on the bare nucleus and the neutral atom are very much alike for not-too-small impact energies. This is explained by the fact that the dominant contribution to the matrix element of the amplitude of the process comes from the small distances of configuration space. At these distances, the continuum-state electron “feels” mainly the bare nuclear charge and the screening effect is relatively small. At larger distances, the continuum-state electron wave function oscillates rapidly, so that the contribution to the radial integral is small. When the impact energy increases, the region of configuration space responsible for the dominant part of the integral shifts towards the nucleus and the screening effect decreases.

For $E = 20$ keV and gold target, the screening reduces the forward-scattering cross section by more than a factor of 2, whereas at energies of a few MeV, it is still a 10% effect. For the Stokes parameters, the screening effect is smaller than for the cross section and stays within 10% even at the lowest energy studied, $E = 20$ keV. We observe that for energies below 20 keV and gold target, calculations of the cross section within the screening-potential approximation rapidly become meaningless as the screening effect tends to grow very fast as the energy decreases. On the contrary, the Stokes parameters turn out to be much less sensitive to the electronic structure of the target. We also find that for the high energies above 1 MeV, the screening effect is significant mainly for the cross section at close-to-zero angles, where it amounts to about 10%.

It is interesting to observe that the dependence of the forward-scattering cross section on the impact energy in the tip region is drastically different for the low- Z (carbon) and high- Z (gold) targets. This difference is studied in more detail in Fig. 4. We observe that for carbon, the forward-scattering cross section at the tip nearly vanishes for large range of impact energies, as could be expected from the nonrelativistic theory. On the contrary, the gold target corresponds to the highly relativistic regime and its forward-scattering cross section is strongly non-zero for all energies. At high impact energies $E > 0.5$ MeV, the forward-scattering cross section grows rapidly with the increase of E , whereas the angular distribution of the cross section becomes localized at the increasingly smaller regions near the forward direction.

In Fig. 5, we study the energy dependence of the Stokes parameter P_1 , the only nonvanishing Stokes parameter for the initially unpolarized electrons. We observe that the shape of the angular distribution of P_1 depends strongly on the energy of the initial electron E . For small E , P_1 tends to its nonrelativistic value of $P_1 = 1$, whereas for the increasingly larger energies, maximum of the angular distribution decreases and shifts towards the forward direction and its tail crosses the zero axis (the “crossover” feature [8]). On the contrary, when the initial energy E is fixed and the energy of the final electron is varied, the shape of the angular distribution stays much the same but its amplitude decreases.

In Fig. 6, we plot the Stokes parameter P_1 as a function of the fractional energy carried away by the photon, k/E , for two targets, carbon and gold, and for two values of the angle of the emitted photon. These plots correspond to the experiment that is currently underway in TU Darmstadt [15].

We now turn to the case of the initially polarized electrons. In the present investigation, we restrict ourself to studying the longitudinal polarization. Fig. 7 presents our results for the Stokes parameters P_2 and P_3 as functions of the initial energy E and of the energy of the final-state electron. (We recall that P_1 for the longitudinally polarized electrons is the same as for the unpolarized ones and shown in Fig. 5.) The Stokes parameter P_2 is of pure relativistic origin and thus is very small for small initial energies. With increase of E , P_2 becomes comparable to P_1 , has its maximum at about $E = 1$ MeV, and then gradually decreases. The third Stokes parameter P_3 is also a relativistic effect and thus vanishes for small initial energies. However, in the high-energy region and $k/E \sim 1$, P_3 changes its behaviour drastically and approaches unity everywhere except for the backward direction.

VI. SUMMARY

In this paper, we report a detailed study of the electron-atom bremsstrahlung process within the rigorous relativistic approach based on the partial-wave expansion of the Dirac wave functions in the external atomic field. Assuming that the final-state electron is not observed, we evaluate the double-differential cross section and all polarization correlations. Unlike in the previous studies, our description of the polarization correlations is formulated entirely in terms of the Stokes parameters, which are directly related to quantities observed in modern experiments. For our calculations, we developed an efficient and reliable scheme of evaluation of the radial integrals for the free-free transitions, based on the complex-plane rotation of the integration contour. The method is applied for the Dirac solutions in both the point-Coulomb potential and the finite-range screening potential.

The numerical procedure was carefully checked by

comparing our results against those reported in the literature. Comparison of our results obtained for the hard-photon end point of the bremsstrahlung spectrum with the extrapolation of the radiative recombination results yielded a numerical proof of the connection between bremsstrahlung and radiative recombination and served as an additional check of our computational scheme.

The numerical results reported present a detailed analysis of (i) the screening effect induced by the electrons of the target on the cross section and polarization correlations and (ii) the energy dependence of the polarization correlations, with the main focus on the high-energy region, which is of primary interest in the future experiments at GSI. We conclude that the tip region of

the bremsstrahlung spectrum is the most appropriate for studying the polarization correlations, as all polarization correlations have their maximum values there.

Acknowledgement

The authors are grateful to Prof. R. Pratt for valuable and interesting discussions. Help of Dr. L. Sharma in using the GRASP package is acknowledged. The work reported in this paper was supported by the Helmholtz Gemeinschaft (Nachwuchsgruppe VH-NG-421).

-
- [1] A. V. Korol, O. I. Obolensky, A. V. Solov'ov, and I. A. Solovjev, *J. Phys. B* **34**, 1589 (2001).
 [2] J. D. Rozics and W. R. Johnson, *Phys. Rev.* **135**, B56 (1964).
 [3] H. Brysk, C. D. Zerby, and S. K. Penny, *Phys. Rev.* **180**, 104 (1969).
 [4] H. K. Tseng and R. H. Pratt, *Phys. Rev. A* **3**, 100 (1971).
 [5] H. K. Tseng and R. H. Pratt, *Phys. Rev. Lett.* **33**, 516 (1974).
 [6] C. M. Lee, R. H. Pratt, and H. K. Tseng, *Phys. Rev. A* **16**, 2169 (1977).
 [7] H. K. Tseng and R. H. Pratt, *Phys. Rev. A* **19**, 1525 (1979).
 [8] H. K. Tseng and R. H. Pratt, *Phys. Rev. A* **7**, 1502 (1973).
 [9] C. D. Shaffer, X.-M. Tong, and R. H. Pratt, *Phys. Rev. A* **53**, 4158 (1996).
 [10] S. Keller and R. M. Dreizler, *J. Phys. B* **30**, 3257 (1997).
 [11] H. K. Tseng, *J. Phys. B* **35**, 1129 (2002).
 [12] W. Nakel, *Phys. Rep.* **243**, 317 (1994).
 [13] S. Tashenov, T. Stöhlker, D. Banaś, K. Beckert, P. Beller, H. F. Beyer, F. Bosch, S. Fritzsche, A. Gumberidze, S. Hagmann, C. Kozhuharov, T. Krings, D. Liesen, F. Nolden, D. Protic, D. Sierpowski, U. Spillmann, M. Steck, and A. Surzhykov, *Phys. Rev. Lett.* **97**, 223202 (2006).
 [14] S. Tashenov et al., in preparation.
 [15] R. Martin et al., Proceedings of CAARI conference, 2010, to be published.
 [16] V. Balashov, A. Grum-Grzhimailo, and N. Kabachnik, *Polarization and Correlation Phenomena in Atomic Collisions* (Kluwer Academic/Plenum, NY, 2000).
 [17] J. Eichler and T. Stöhlker, *Phys. Rev.* **439**, 1 (2007).
 [18] M. E. Rose, *Relativistic Electron Theory* (John Wiley, NY, 1961).
 [19] D. A. Varshalovich, A. N. Moskalev, and V. K. Khersonskii, *Quantum Theory of Angular Momentum* (World Scientific, Singapore, 1988).
 [20] J. J. Dugne and J. Proriol, *Phys. Rev. A* **12**, 842 (1975).
 [21] H. K. Tseng, PhD thesis, University of Pittsburgh, unpublished, 1970.
 [22] C. M. Vincent and H. T. Fortune, *Phys. Rev. C* **2**, 782 (1970).
 [23] K. T. R. Davies, M. R. Strayer, and G. D. White, *J.*

TABLE I: Comparison of the results of the present calculation of the bremsstrahlung cross section $\sigma(k)$ with that by Tseng and Pratt [4], for the gold target ($Z = 79$) and the Coulomb and screening potentials, in mbarn. E is the kinetic energy of the incoming electron and k is the energy of the emitted photon.

E [MeV]	k/E	This work		Ref. [4]	
		Coulomb	screened	Coulomb	screened
0.050	0.6	42.61	42.59	35.06	35.62
	0.4	46.74	46.72	36.92	37.29
0.180	0.6	14.68	14.67	13.22	13.34
	0.6	8.555	8.522	7.884	7.942
0.500	0.96	4.791	4.789	4.463	4.526
	0.5	8.201	8.142	7.562	7.600

- Phys. G* **14**, 961 (1988).
 [24] N. C. Sil, M. A. Crees, and M. J. Seaton, *J. Phys. B* **17**, 1 (1984).
 [25] S. Keller, C. T. Whelan, H. Ast, H. R. J. Walters, and R. M. Dreizler, *Phys. Rev. A* **50**, 3865 (1994).
 [26] P. M. Bergstrom, T. Surić, K. Pisk, and R. H. Pratt, *Phys. Rev. A* **48**, 1134 (1993).
 [27] F. Salvat, J. M. Fernández-Varea, and W. Williamson Jr., *Comput. Phys. Commun.* **90**, 151 (1995).
 [28] V. A. Yerokhin and V. M. Shabaev, *Phys. Rev. A* **60**, 800 (1999).
 [29] F. A. Parpia, C. Froese Fischer, and I. P. Grant, *Comput. Phys. Commun.* **94**, 249 (1996).
 [30] U. Fano, *Phys. Rev.* **116**, 1156 (1959).
 [31] C. M. Lee and R. H. Pratt, *Phys. Rev. A* **12**, 1825 (1975).
 [32] I. J. Feng, I. B. Goldberg, Y. S. Kim, and R. H. Pratt, *Phys. Rev. A* **28**, 609 (1983).
 [33] D. H. Jakubassa-Amundsen, *Phys. Rev. A*, in press.
 [34] R. H. Pratt and H. K. Tseng *Phys. Rev. A* **11**, 1797 (1975).
 [35] A. Surzhykov, S. Fritzsche, T. Stöhlker, and S. Tashenov, *Phys. Rev. A* **68**, 022710 (2003).
 [36] J. Eichler and W. Meyerhof, *Relativistic Atomic Collisions* (Academic Press, San Diego, 1995).
 [37] I. Gradshteyn and I. Ryzhik, *Table of Integrals, Series and Products* (Academic Press, NY, 1994).

Appendix A: Reduced matrix elements

Results for the reduced matrix elements in Eq. (18) are

$$(-i)\langle \varepsilon_a \kappa_a || \boldsymbol{\alpha} \cdot \mathbf{a}_l^{(0)} || \varepsilon_b \kappa_b \rangle = J_l^{12}(a, b) s_{ll}(\kappa_a, -\kappa_b) - J_l^{21}(a, b) s_{ll}(-\kappa_a, \kappa_b), \quad (\text{A1})$$

$$\begin{aligned} (-i)\langle \varepsilon_a \kappa_a || \boldsymbol{\alpha} \cdot \mathbf{a}_l^{(1)} || \varepsilon_b \kappa_b \rangle &= \sqrt{\frac{l+1}{2l+1}} \left[J_{l-1}^{12}(a, b) s_{l, l-1}(\kappa_a, -\kappa_b) - J_{l-1}^{21}(a, b) s_{l, l-1}(-\kappa_a, \kappa_b) \right] \\ &\quad - \sqrt{\frac{l}{2l+1}} \left[J_{l+1}^{12}(a, b) s_{l, l+1}(\kappa_a, -\kappa_b) - J_{l+1}^{21}(a, b) s_{l, l+1}(-\kappa_a, \kappa_b) \right], \end{aligned} \quad (\text{A2})$$

where the angular coefficients are given by

$$s_{LJ}(\kappa_1, \kappa_2) = \langle \kappa_1 || \boldsymbol{\sigma} \cdot \mathbf{Y}_{LJ} || \kappa_2 \rangle = \langle \kappa_1 || [Y_J \otimes \boldsymbol{\sigma}]_L || \kappa_2 \rangle = \sqrt{\frac{3}{2\pi}} (-1)^{l_2} [j_1, j_2, l_1, l_2, L]^{1/2} C_{l_1 0, l_2 0}^{J 0} \begin{Bmatrix} j_1 & l_1 & 1/2 \\ j_2 & l_2 & 1/2 \\ L & J & 1 \end{Bmatrix}, \quad (\text{A3})$$

\mathbf{Y}_{JLM} are the vector spherical harmonics defined by Eq. (17) and the radial integrals $J_l^{12}(a, b)$ and $J_l^{21}(a, b)$ are defined by Eqs. (30) and (31).

Appendix B: Free-free integrals: Coulomb case

We need the radial integrals of the form

$$J_l^{ij}(\varepsilon_1, \kappa_1, \varepsilon_2, \kappa_2) = \int_0^\infty dr r^2 f_{\varepsilon_1, \kappa_1, i}(r) f_{\varepsilon_2, \kappa_2, j}(r) j_l(kr), \quad (\text{B1})$$

where j_l is the spherical Bessel function, $k = |\varepsilon_1 - \varepsilon_2|$, and $f_{\varepsilon, \kappa, 1} \equiv g_{\varepsilon, \kappa}$ and $f_{\varepsilon, \kappa, 2} \equiv f_{\varepsilon, \kappa}$ are the upper and the lower radial components of the Dirac wave function. In the following, we will assume that $\varepsilon_1 > \varepsilon_2 \geq m$, which entails that $p_1 - p_2 - k > 0$, where $p_i = \sqrt{\varepsilon_i^2 - m^2}$. By this restriction, we exclude the possibility $\varepsilon_1 = \varepsilon_2$, in which case the method described in this section is not applicable.

For $\varepsilon > m$, the radial components of the Dirac-Coulomb wave functions normalized on the energy scale are given by [36]:

$$g_{\varepsilon, \kappa}(r) = N_\kappa \sqrt{\varepsilon + 1} (2pr)^{-3/2} \text{Re} \left\{ e^{i[\delta_\kappa - \frac{\pi}{2}(\gamma + \frac{1}{2})]} \times (\gamma + i\eta) M_{-1/2 - i\eta, \gamma}(2ipr) \right\}, \quad (\text{B2})$$

$$f_{\varepsilon, \kappa}(r) = -N_\kappa \sqrt{\varepsilon - 1} (2pr)^{-3/2} \text{Im} \left\{ e^{i[\delta_\kappa - \frac{\pi}{2}(\gamma + \frac{1}{2})]} \times (\gamma + i\eta) M_{-1/2 - i\eta, \gamma}(2ipr) \right\}, \quad (\text{B3})$$

where $p = \sqrt{\varepsilon^2 - m^2}$, $\eta = Z\alpha\varepsilon/p$, $\gamma = \sqrt{\kappa^2 - (Z\alpha)^2}$,

$$N_\kappa = 2\sqrt{\frac{p}{\pi}} e^{\pi\eta/2} \frac{|\Gamma(\gamma + i\eta)|}{\Gamma(2\gamma + 1)}, \quad (\text{B4})$$

$$e^{2i\delta_\kappa} = \frac{-\kappa + i\eta/\varepsilon}{\gamma + i\eta}, \quad (\text{B5})$$

and $M_{\alpha, \beta}$ is the Whittaker function of the first kind [37].

It is clear that the integrals J_l^{ij} can be expressed in terms of the integrals involving two Whittaker functions and a Bessel function,

$$I_{\alpha_1, \gamma_1, \alpha_2, \gamma_2, l}(p_1, p_2, k) = \int_0^\infty dr r^{-1} M_{\alpha_1, \gamma_1}(2ip_1 r) \times M_{\alpha_2, \gamma_2}(2ip_2 r) j_l(kr), \quad (\text{B6})$$

with the momenta satisfying the condition $p_1 - p_2 - k > 0$. The integrand is highly oscillatory and slowly decreasing function for large values of r , so a straightforward numerical evaluation of this integral up to a high accuracy is practically impossible. The method used in the present work [23] is based on the analytical continuation of the integrand into the complex r plane. More specifically, the integrand is separated into two parts which decrease exponentially in the upper or lower half of the complex plane. By appropriate rotations of the integration contour, the original oscillating integrand can be converted into two smoothly decreasing ones. The resulting integrals can be easily calculated by Gauss-Legendre quadratures up to typically 9 digit accuracy.

To realize this algorithm, we represent the first Whittaker function in the right-hand-side of Eq. (B6) in terms

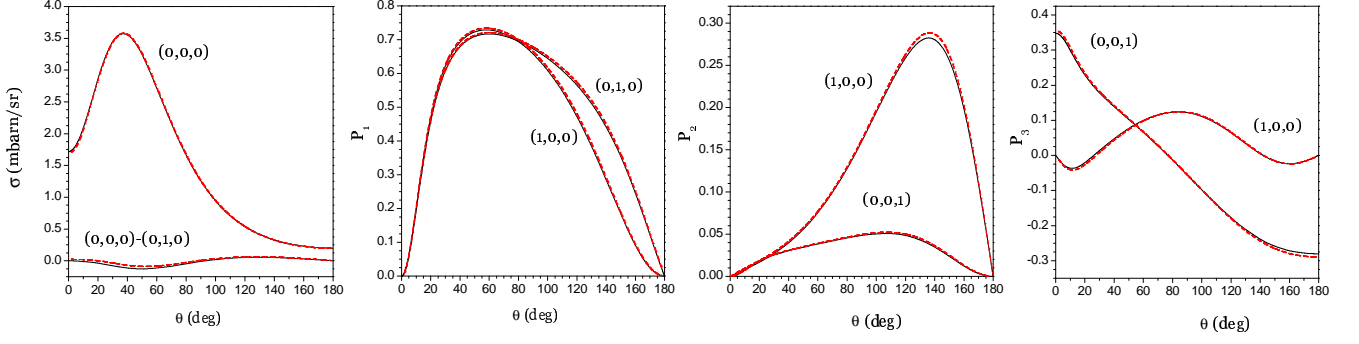


FIG. 1: (Color online) Comparison of the bremsstrahlung at the hard photon end of the spectrum (solid line, black) with the continuum-threshold extrapolation of the radiative recombination (dashed line, red), for the double differential cross section $(k/Z^2) d\sigma/(dk d\Omega_k)$ and the Stokes parameters. Calculations are performed for $Z = 79$, $E = 100$ keV, and the point-nucleus Coulomb potential.

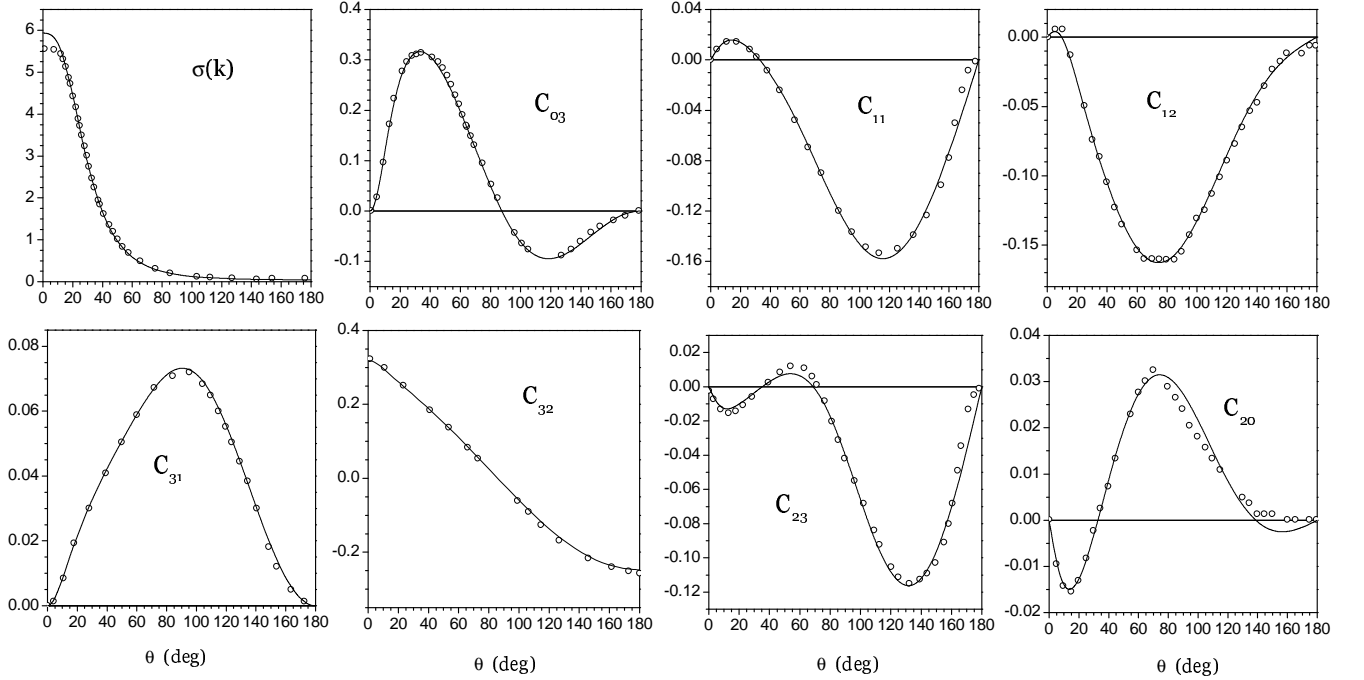


FIG. 2: Comparison of the present results (solid line) with those by Tseng and Pratt [4, 8] (open circles) for the double differential cross section $(k/Z^2) d\sigma/(dk d\Omega_k)$ for the initially unpolarized electrons, in mbarn/sr, and for the polarization correlations C_{ij} . The calculations are performed for $Z = 79$, $E = 500$ keV, $k = 250$ keV, and the point-nucleus Coulomb potential.

of the Whittaker functions of the second kind [37]

$$M_{\alpha,\beta}(z) = \frac{\Gamma(2\beta+1)}{\Gamma(\beta-\alpha+1/2)} e^{i\pi s\alpha} W_{-\alpha,\beta}(-z) + \frac{\Gamma(2\beta+1)}{\Gamma(\beta+\alpha+1/2)} e^{i\pi s(\alpha-\beta-1/2)} W_{\alpha,\beta}(z), \quad (\text{B7})$$

where $s = 1$ if $\text{Im}(z) < 0$ and -1 otherwise. For $r = R + iz$, the asymptotic behavior of the Whittaker and

Bessel functions (for p and $k > 0$ and $|z| \rightarrow \infty$) is

$$M_{\alpha,\beta}(2ipr) \sim e^{p|z|}, \quad W_{\alpha,\beta}(2ipr) \sim e^{pz}, \quad j_l(kr) \sim e^{k|z|}, \quad (\text{B8})$$

where only the leading exponential behavior is kept. These results, together with the condition on the momenta, $p_1 > p_2 + k$, show that the representation (B7) applied to the Whittaker function with the largest momenta $M_{\alpha_1,\gamma_1}(2ip_1r)$, splits the integrand of Eq. (B6) into two parts, one of which [with $W_{-\alpha_1,\gamma_1}(-2ip_1r)$] is regular in the upper half of the complex r plane and the

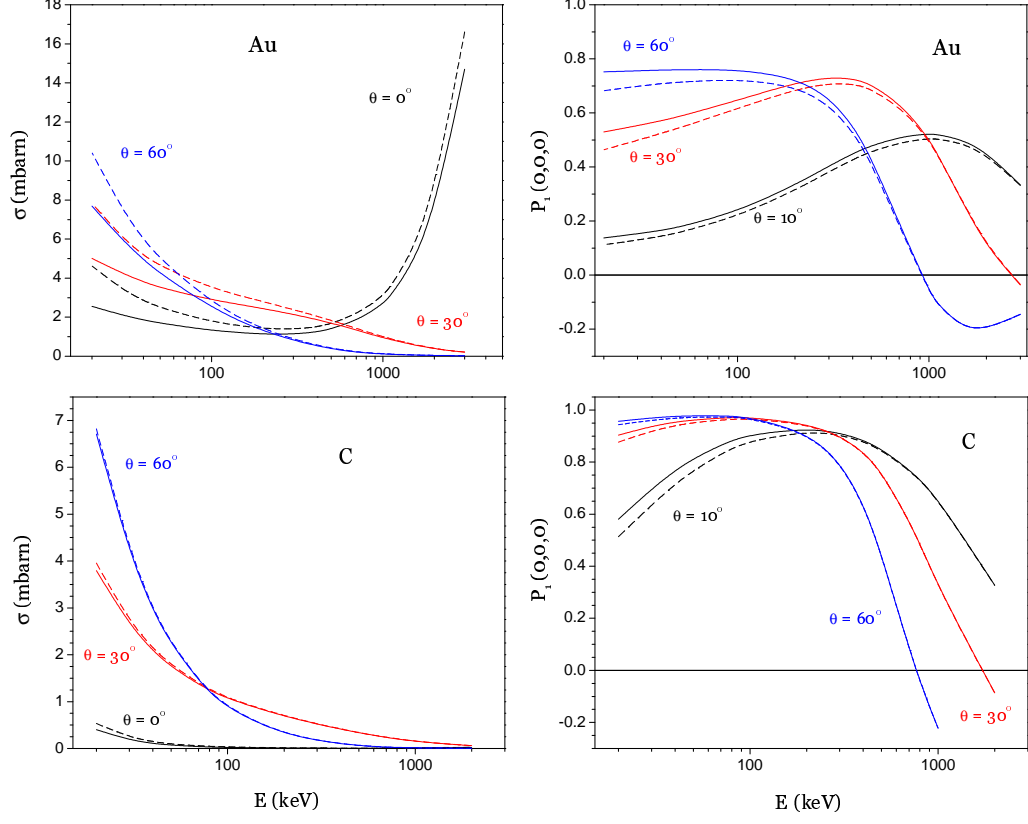


FIG. 3: (Color online) Double differential cross section $(k/Z^2) d\sigma/(dk d\Omega_k)$ and the Stokes parameter P_1 for several angles of the emitted photon θ , as functions of the kinetic energy of the incoming electron E , for gold (upper row) and carbon (lower row) targets, for the Coulomb (dashed line) and screened (solid line) potentials. For all graphs, the kinetic energy of the final electron is $E_f = 1$ keV and initially unpolarized electrons are taken.

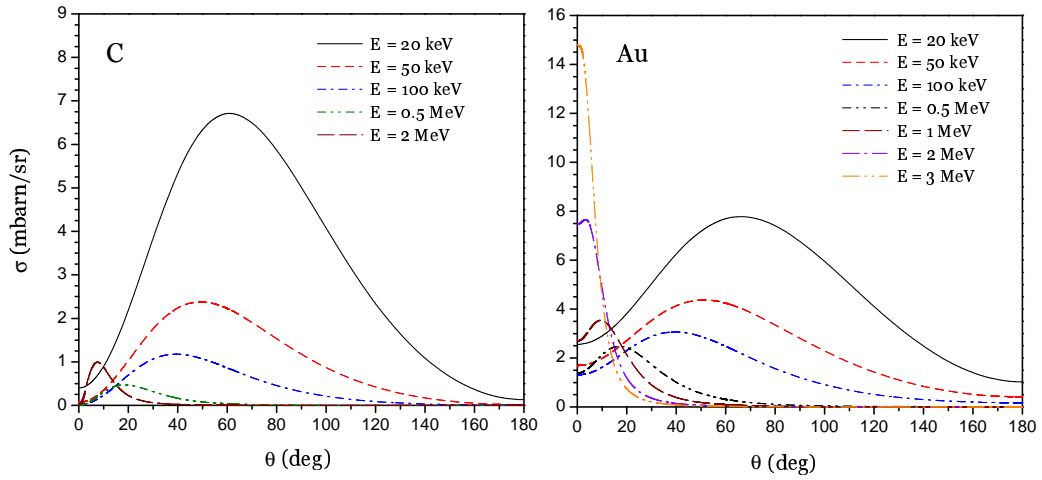


FIG. 4: (Color online) Double differential cross section $(k/Z^2) d\sigma/(dk d\Omega_k)$ for different values of the kinetic energy of the incoming electron E , for neutral carbon (left) and gold (right) targets. Kinetic energy of the final electron is $E_f = 1$ keV and initially unpolarized electrons are taken.

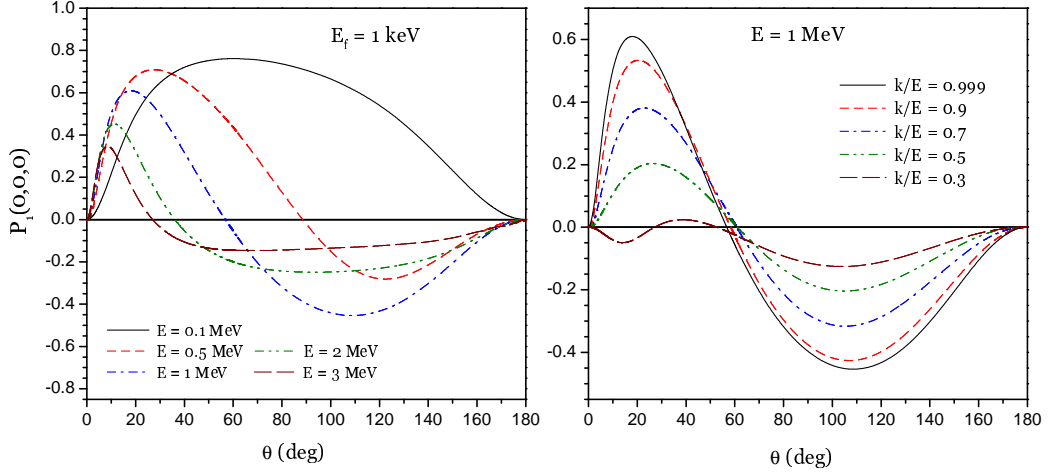


FIG. 5: (Color online) Stokes parameter P_1 for the neutral gold target and initially unpolarized electrons. Left panel contains plots for different values of the kinetic energy of the incoming electron E and the kinetic energy of the final-state electron fixed by $E_f = 1$ keV. In right panel, the initial energy is fixed by $E = 1$ MeV and the final-state energy is varied.

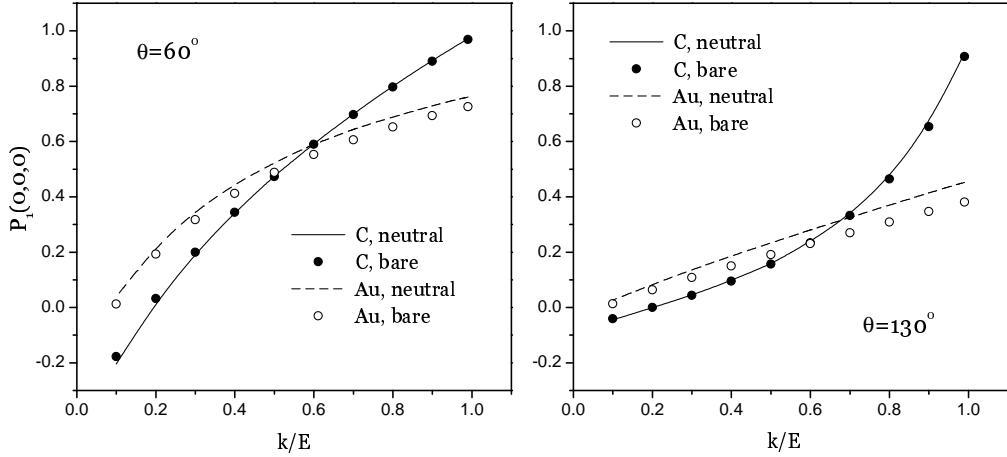


FIG. 6: Stokes parameter P_1 for the initially unpolarized electrons with $E = 100$ keV, for different values of the energy k and the angle θ of the emitted photon, for gold and carbon targets and for the Coulomb and screening potentials.

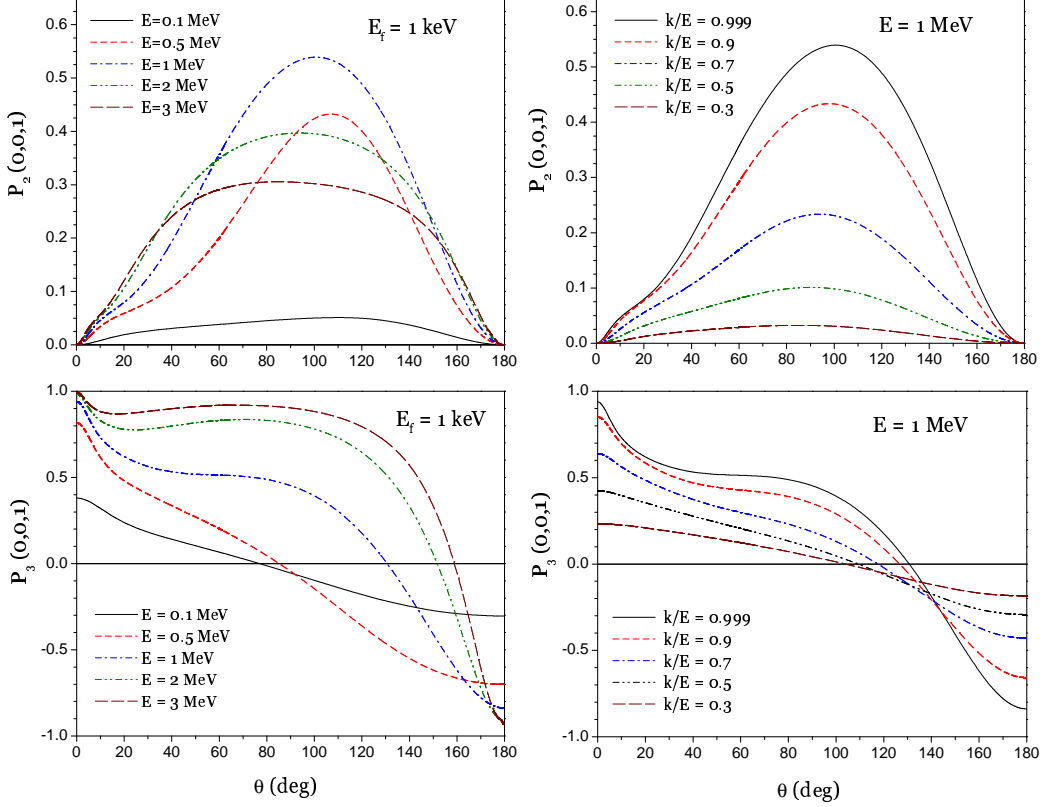


FIG. 7: (Color online) The same as Fig. 5 but for the Stokes parameters P_2 (upper row) and P_3 (lower row) and for the initially longitudinally polarized electrons.

other [with $W_{\alpha_1, \gamma_1}(2ip_1 r)$] is regular into the lower half-plane. In both cases, the resulting integrand falls off as $\sim e^{-(p_1 - p_2 - k)|z|}$, which makes possible accurate numerical evaluation of the corresponding integrals.

In actual calculations, one should keep in mind that Eq. (B7) represents the regular (for small z) function M in terms of the irregular functions W . Because of this, it is advantageous to integrate Eq. (B6) along the real axis up to a certain value of $r = R$ and to perform the rotation of the integration contour for $r > R$. So, Eq. (B6) is represented as

$$I = \int_0^R dr I(r) + \int_0^\infty dz i [I_+(R + iz) - I_-(R - iz)], \quad (\text{B9})$$

where $I(r)$ stands for the integrand of the right-hand-side of Eq. (B6), and $I_+(r)$ and $I_-(r)$ are the parts of $I(r)$ regular in the upper and lower half-plane, respectively, $I(r) = I_+(r) + I_-(r)$.

Appendix C: Free-free integrals: neutral atom

We now consider the potential in the Dirac equation to be a finite-range screening potential (having in mind

a neutral atomic system),

$$V(r) = V_{\text{scr}}(r), \quad (\text{C1})$$

where $V_{\text{scr}}(r) = 0$ for $r \geq R_0$. In this case, in the outer region $r \geq R_0$, the solutions of the Dirac equation can be expressed in terms of the free Dirac eigenfunctions, given by

$$g_{\varepsilon, \kappa}^{(0)}(r) = \sqrt{\frac{p(\varepsilon + 1)}{\pi}} \left[j_l(pr) \cos \delta - y_l(pr) \sin \delta \right], \quad (\text{C2})$$

$$f_{\varepsilon, \kappa}^{(0)}(r) = \frac{|\kappa|}{\kappa} \sqrt{\frac{p(\varepsilon - 1)}{\pi}} \left[j_{\bar{l}}(pr) \cos \delta - y_{\bar{l}}(pr) \sin \delta \right], \quad (\text{C3})$$

where j_l and y_l are the spherical Bessel and Neumann functions, respectively; $l = |\kappa + 1/2| - 1/2$, $\bar{l} = |\kappa - 1/2| - 1/2$, and δ is the scattering phase shift induced by the finite-range potential V_{scr} and determined by the matching procedure at $r = R_0$. (In the absence of any field, $\delta = 0$.) Note that the definition of the overall sign in the wave functions agrees with that of Ref. [36]. The definition used in Ref. [27] differs from the present one by a factor of $-\kappa/|\kappa|$.

For the evaluation of radial integrals, it is convenient to express the free Dirac eigenfunctions in terms of the spherical Hankel functions of the first and second kind ($h_l^{(1)}$ and $h_l^{(2)}$, respectively),

$$g_{\varepsilon,\kappa}^{(0)}(r) = \sqrt{\frac{p(\varepsilon+1)}{\pi}} \frac{1}{2} \left[h_l^{(1)}(pr) e^{i\delta} + h_l^{(2)}(pr) e^{-i\delta} \right], \quad (\text{C4})$$

$$f_{\varepsilon,\kappa}^{(0)}(r) = \frac{|\kappa|}{\kappa} \sqrt{\frac{p(\varepsilon-1)}{\pi}} \frac{1}{2} \left[h_l^{(1)}(pr) e^{i\delta} + h_l^{(2)}(pr) e^{-i\delta} \right]. \quad (\text{C5})$$

Taking into account that $h_l^{(1)}(pr) \sim e^{ipr}$ and $h_l^{(2)}(pr) \sim e^{-ipr}$ as $r \rightarrow \infty$, we conclude that the first terms in the brackets of Eqs. (C4) and (C5) are regular in the upper half of the complex r plane, whereas the second terms are regular in the lower half-plane.

The integral involving the free Dirac eigenfunctions can be evaluated as

$$\begin{aligned} J_l^{ij}(\varepsilon_1, \kappa_1, \varepsilon_2, \kappa_2, R) &= \int_R^\infty dr r^2 f_{\varepsilon_1, \kappa_1, i}^{(0)}(r) f_{\varepsilon_2, \kappa_2, j}^{(0)}(r) j_l(kr) \\ &= \int_0^\infty dz i \left[x^2 f_{\varepsilon_1, \kappa_1, i}^{(0),+}(x) f_{\varepsilon_2, \kappa_2, j}^{(0)}(x) j_l(kx) - x^{*2} f_{\varepsilon_1, \kappa_1, i}^{(0),-}(x^*) f_{\varepsilon_2, \kappa_2, j}^{(0)}(x^*) j_l(kx^*) \right], \end{aligned} \quad (\text{C6})$$

where $x = R + iz$, and superscripts “+” and “-” label the parts of the eigenfunction that are regular in the upper and lower half-plane, respectively. Using the property of the spherical Hankel functions

$$\left[h_l^{(1)}(z) \right]^* = h_l^{(2)}(z^*), \quad (\text{C7})$$

the expression for J_R^{ij} is reduced to

$$\begin{aligned} J_l^{ij}(\varepsilon_1, \kappa_1, \varepsilon_2, \kappa_2, R) &= -2 \text{Im} \int_0^\infty dz x^2 \\ &\quad \times f_{\varepsilon_1, \kappa_1, i}^{(0),+}(x) f_{\varepsilon_2, \kappa_2, j}^{(0)}(x) j_l(kx). \end{aligned} \quad (\text{C8})$$

It can be easily seen that the integrand in the above

expression falls off as $e^{-(p_1 - p_2 - k)z}$ for large z .

For r smaller than the radius of the atom R_0 , the wave functions are obtained numerically by solving the Dirac equation, so this part of the radial integration has to be performed along the real axis. When the energy of the incoming electron becomes large, the integration within the radius of the atom (which is of order of several atomic units) might become troublesome as the integrand is rapidly oscillating. To simplify the numerical evaluation, we exploit the fact that, for heavy atoms, the maximum of the screening potential V_{scr} is localized close to the nucleus. Further away from the maximum, the numerical solutions of the Dirac equation resemble the free asymptotic solutions, so that the difference between them is a smooth, rapidly decreasing function. We thus represent the radial integrals J_l^{ij} [Eq. (B1)] as

$$\begin{aligned} J_l^{ij}(\varepsilon_1, \kappa_1, \varepsilon_2, \kappa_2) &= \int_0^R dr r^2 f_{\varepsilon_1, \kappa_1, i}(r) f_{\varepsilon_2, \kappa_2, j}(r) j_l(kr) \\ &\quad + \int_R^{R_0} dr r^2 \left[f_{\varepsilon_1, \kappa_1, i}(r) f_{\varepsilon_2, \kappa_2, j}(r) - f_{\varepsilon_1, \kappa_1, i}^{(0)}(r) f_{\varepsilon_2, \kappa_2, j}^{(0)}(r) \right] j_l(kr) \\ &\quad - 2 \text{Im} \int_0^\infty dz x^2 f_{\varepsilon_1, \kappa_1, i}^{(0),+}(x) f_{\varepsilon_2, \kappa_2, j}^{(0)}(x) j_l(kx), \end{aligned} \quad (\text{C9})$$

where $x = R + iz$. The free parameter $R < R_0$ is chosen as the smallest distance for which the exact Dirac solution $f_{\varepsilon, \kappa, i}(r)$ resembles the free asymptotic solution $f_{\varepsilon, \kappa, i}^{(0)}(r)$.